

pubs.acs.org/JPCA Article

# Competitive Radical Migrations and Ribose Ring Cleavage in Adenosine and 2'-Deoxyadenosine Cation Radicals

Václav Zima, Aleš Marek, and František Tureček\*



Cite This: J. Phys. Chem. A 2024, 128, 1109-1123



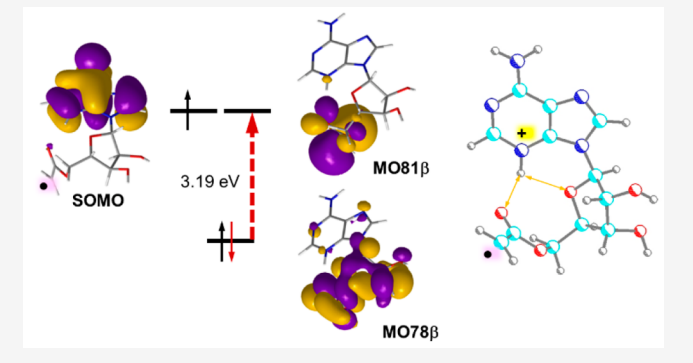
**ACCESS** I

Metrics & More

Article Recommendations

Supporting Information

**ABSTRACT:** We report a combined experimental and computational study of adenosine cation radicals that were protonated at adenine and furnished with a radical handle in the form of an acetoxyl radical, \*CH<sub>2</sub>COO, that was attached to ribose 5'-O. Radicals were generated by collision-induced dissociation (CID) and characterized by tandem mass spectrometry and UV-vis photodissociation action spectroscopy. The acetoxyl radical was used to probe the kinetics of intramolecular hydrogen transfer from the ribose ring positions that were specifically labeled with deuterium at C1', C2', C3', C4', C5', and in the exchangeable hydroxyl groups. Hydrogen transfer was found to chiefly involve 3'-H with minor contributions by 5'-H and 2'-H, while 4'-H was nonreactive. The hydrogen transfer rates were affected by



deuterium isotope effects. Hydrogen transfer triggered ribose ring cleavage by consecutive dissociations of the C4′–O and C1′–C2′ bonds, resulting in expulsion of a  $C_6H_9O_4$  radical and forming a 9-formyladenine ion. Rice-Ramsperger-Kassel-Marcus (RRKM) and transition-state theory (TST) calculations of unimolecular constants were carried out using the effective CCSD(T)/6-311++G(3d,2p) and M06-2X/aug-cc-pVTZ potential energy surfaces for major isomerizations and dissociations. The kinetic analysis showed that hydrogen transfer to the acetoxyl radical was the rate-determining step, whereas the following ring-opening reactions in ribose radicals were fast. Using DFT-computed energies, a comparison was made between the thermochemistry of radical reactions in adenosine and 2′-deoxyadenosine cation radicals. The 2′-deoxyribose ring showed lower TS energies for both the rate-determining 3′-H transfer and ring cleavage reactions.

## ■ INTRODUCTION

The formation of radicals in nucleic acids has been recognized as a major cause of chemical damage, resulting in nucleobase loss and strand breaks. 1-3 Among the major chemical DNA damage processes, electron attachment to DNA oligonucleotides<sup>4</sup> initiates nucleobase loss and generates deoxyribose radicals that can undergo further reactions. 5-8 Attack by hydroxyl radical and other reactive oxygen species can result in hydrogen abstraction, forming deoxyribose radicals that are prone to further reactions. 9,10 The formation of nucleotide sugar radicals by photoexcitation of ionized guanosine has been studied in solution and frozen glasses using electron paramagnetic resonance spectroscopy (EPR).<sup>11</sup> However, the mechanism and energetics of the radical formation have not been addressed except for simplified models. 12-14 Interstrand hydrogen atom abstraction has been reported to cause double-strand cleavage in DNA. 15 Hydrogen atom abstraction from ribose and thymidine by distonic phenyl cation radicals has been studied in the gas phase; however, the nature of the neutral radicals has not been determined. 16 Studies that have been aimed at the generation of cation radicals of nucleic acid components in the gas phase have addressed nucleobases, nucleosides, and oligonucleotides, as reviewed. In particular, hydrogen atom transfers in oligonucleotide cation radicals have been detected by tandem mass spectrometry that was coupled to UV—vis photodissociation action spectroscopy (UVPD) of gas-phase ions. <sup>18–24</sup> O'Hair and co-workers have used infrared multiphoton dissociation (IRMPD) spectroscopy to characterize the cytosine—guanosine Watson—Crick pair as a cation radical in the gas phase. These authors have also provided density-functional theory (DFT) calculations to rationalize the observed dissociations. <sup>25</sup>

Here, we report the use of an intrinsic radical initiator to generate ribose radicals in adenosine ions. Covalently attached radical initiators have been used to produce peptide and carbohydrate radicals in gas-phase ions to facilitate sequencing and structure analysis.  $^{26,27}$  In a general scheme, the biomolecule of interest is furnished with a functional group (R) and nondestructively ionized by protonation or other cation

Received: December 3, 2023 Revised: January 15, 2024 Accepted: January 17, 2024 Published: February 5, 2024





attachment to form gas-phase ions (Scheme 1). Collisional excitation <sup>26,27</sup> or electron transfer<sup>28</sup> is then used to convert the

Scheme 1. Radical Initiator

R Biomolecule 
$$HOOC$$
 $R$ 
 $H_3C$ 
 $CN$ 
 $H_3C$ 
 $H_3C$ 

substituent to a reactive initiator  $(I_r)$  that triggers radical reactions in the biomolecule yielding dissociation products that can be analyzed by tandem mass spectrometry. As an initiator, we used the 4,4'-azo(4-cyanopentanoyl)(4'-cyanopentanoic acid) group<sup>26</sup> that can be readily attached as an ester or amide. Collision-induced dissociation (CID) results in a multistep formation of an acetyl radical that remains attached to the biomolecule where it can initiate hydrogen atom transfer accompanied by dissociation. We have used this method previously for cascade dissociations yielding unusual isomers of adenine and guanine cation radicals.<sup>29</sup> Here, we employ the radical initiator method to generate ribose radicals in adenosine ions that are investigated by specific deuterium labeling, tandem mass spectrometry, and UVPD. Experimental work is

complemented by ab initio and DFT calculations providing cation radical structures, energies, rate constants, and theoretical absorption spectra.

## **■ EXPERIMENTAL SECTION**

**Materials.** Adenosines labeled with deuterium in positions 1', 2', and 5' were purchased from Cambridge Isotope Laboratories, Inc. (Andover, MA, USA), and the 4'-D labeled adenosine was purchased from AX Molecules (San Marcos, CA, USA). Adenosine labeled with deuterium at C3' was synthesized according to Scheme S1 (Supporting Information). The reagents and reaction conditions are described in detail in the Supporting Information. All adenosine conjugates esterified at 5'-O with 4,4'-azobis(4-cyanopentanoic acid) were prepared in three steps according to Scheme 2. Detailed procedures for all compounds and product characterization by <sup>1</sup>H and <sup>13</sup>C NMR and high-resolution mass spectrometry are described in the Supporting Information (Figures S1–S13, Scheme S1).

**Methods.** Tandem mass spectra were measured on a Bruker amaZon ion trap mass spectrometer that was furnished with laser optics for photodissociation action spectroscopy. The light beam from an NL301G (Altos Photonics, Bozeman, MT, USA) Nd:YAG laser operating at 20 Hz was directed into a PG142C unit that consisted of a third-harmonic generator and an optical parametric oscillator that was coupled to an optional second-harmonic generator. The wavelength was scanned in 2 nm steps over two sections that spanned the 210–354 and 355–409 nm regions and in 5 nm steps in the third region of 410–700 nm. The laser pulse energies, which typically ranged between 0.2 and 4.0 mJ, were measured at each wavelength to calibrate the action spectra. Samples were dissolved in methanol:water:acetic acid 50:50:1 and electrosprayed to produce ions.

High-resolution mass spectra were measured on an Orbitrap Ascend Tribrid instrument (ThermoFisher, San Jose, CA) at a 100 000 resolving power. The accurate masses and ion formulas are in Table S1 (Supporting Information).

Scheme 2. Preparation of Adenosine Conjugates<sup>a</sup>

<sup>&</sup>lt;sup>a</sup>The reagents were as follows: i – acetone, p-toluenesulfonic acid; ii – 4,4′-azobis(4-cyanopentanoic acid), N,N-dimethylaminopyridine, dicyclohexylcarbodiimide, acetonitrile; iii – trifluoroacetic acid—water, 1:1.

Scheme 3. Generation of Adenosine Cation Radicals by CID-MS<sup>n</sup>

**Calculations.** Ion conformations were obtained by Born-Oppenheimer molecular dynamics (BOMD) calculations as described previously.<sup>29</sup> BOMD trajectories (20 ps) were run in 1 fs steps under the high-level Cuby4 platform<sup>31</sup> with the semiempirical PM6 method<sup>32</sup> that was augmented by including hydrogen bonding and dispersion interactions (D3H4)<sup>33</sup> and run under MOPAC.<sup>34</sup> Energy balance was maintained with the Berendsen thermostat.<sup>35</sup> 200 structures were selected at regular intervals from the 20 000 snapshots in each trajectory, and their geometries were fully optimized with PM6-D3H4. Geometries of selected low-energy structures were then reoptimized with  $B3LYP^{36}$  and  $M06-2X^{37}$  and the 6-31+G(d,p) basis set. Calculations of open-shell systems were performed with the spin-unrestricted formalism. These calculations also provided harmonic frequencies to characterize local energy minima and first-order saddle points. The M06-2X-optimized geometries were used for single-point energy calculations that were run at several levels. One set of single-point energies was obtained by M06-2X with the aug-cc-pVTZ basis set.<sup>38</sup> These were compared with M06-2X relative energies that were calculated with the def2TZVPP and def2QZVPP basis sets, <sup>39,40</sup> which gave essentially identical results with the M06-2X/aug-cc-pVTZ data, showing root-mean square differences of 0.5 and 1.3 kJ mol respectively (Table S2, Supporting Information). Another set of energies were obtained by Møller-Plesset calculations (MP2 frozen core) $^{41}$  with the 6-311++G(3df,2p) basis set. These were combined with coupled-clusters calculations 42 with single, double, and disconnected triple excitations<sup>43</sup> (CCSD(T)) that were performed with the 6-31G(d,p) basis set. The MP2 and CCSD(T) energies were combined<sup>44</sup> to provide estimated CCSD(T) energies as  $E[CCSD(T)/6-311++G(3df,p)] \approx$ E[CCSD(T)/6-31G(d,p)] + E[MP2/6-311++G(3df,2p)] -E[MP2/6-31G(d,p)]. All standard ab initio and DFT calculations were run with Gaussian 16 (revision B.01) that was licensed from Gaussian, Inc. (Wallingford, CT). Unimolecular rate constants for isomerizations and dissociations were obtained using Rice-Ramsperger-Kassel-Marcus (RRKM) calculations<sup>45</sup> that were run with the QP program<sup>46</sup> that was recompiled for MS-DOS and run under Windows.<sup>47</sup> Excitedstate calculations were carried out with time-dependent DFT (TD-DFT), 48 using M06-2X/6-31+G(d,p). Previous comparisons with equation-of-motion coupled-clusters calculations have established that M06-2X/6-31+G(d,p) excitation energies in cation radicals were within 0.1-0.2 eV of the benchmark values. 49,50 No corrections were applied to the calculated excitation energies and oscillator strengths. To calculate vibronic absorption spectra, we used normal coordinates obtained from vibrational analysis to generate Wigner configurations<sup>51,52</sup> at

310–350 K that were sorted out by their Boltzmann factors. Three hundred selected lowest-energy configurations were used for TD-DFT calculations of 25-30 excited states that covered the experimental wavelength range down to 200 nm. These calculations were run under Newton  $X^{53}$ 

## ■ RESULTS AND DISCUSSION

**Ion Dissociations.** Adenosine ions carrying the reactive 5′-O-acetyl radical were generated by the reaction sequence shown in Scheme 3. Precursor conjugates, which were furnished with the 4,4′-azo(4-cyanopentanoyl)(4′-cyanopentanoic acid) radical initiator group attached as an ester at the 5′-O ribose

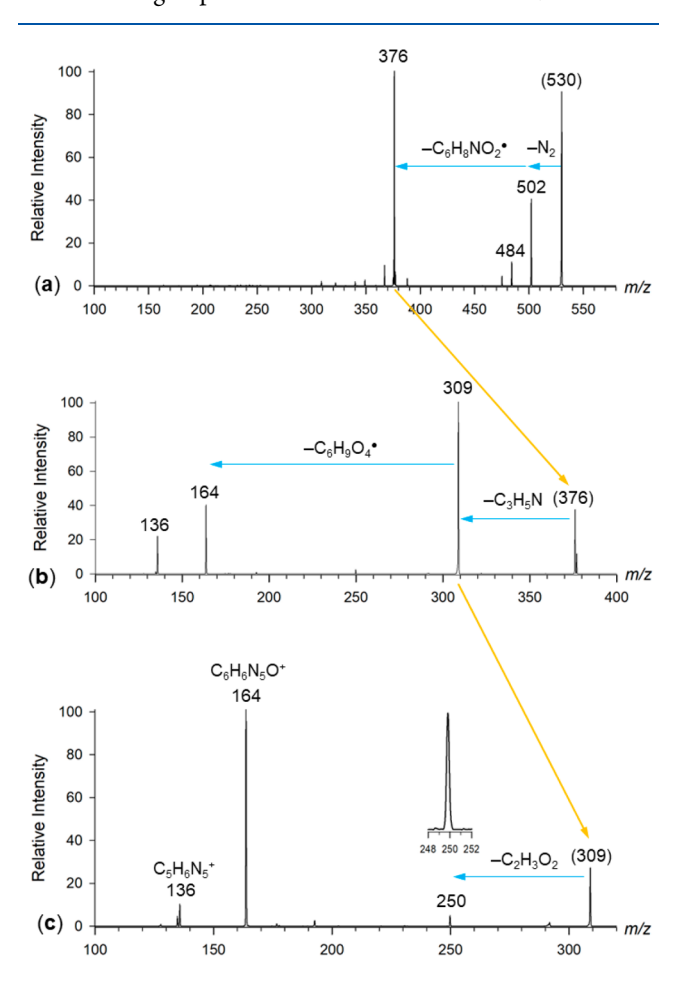


Figure 1. CID-MS<sup>n</sup> spectra of (a)  $(1 + H)^+$  at m/z 530; (b) fragment ion by loss of N<sub>2</sub> and C<sub>6</sub>H<sub>8</sub>NO<sub>2</sub> $^{\bullet}$  (m/z 376); (c) radical 2<sup>+•</sup> at m/z 309.

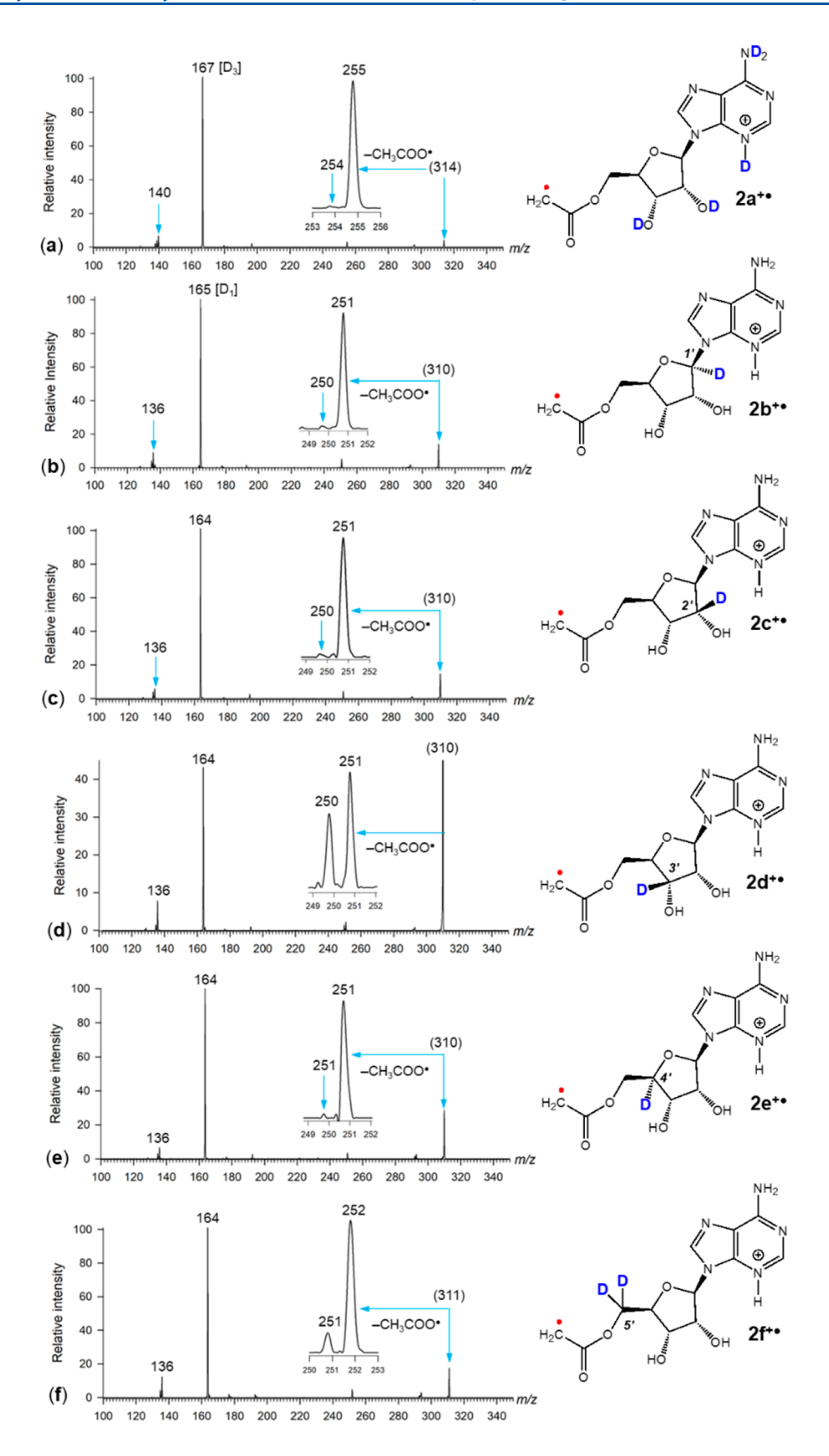


Figure 2. CID-MS<sup>4</sup> of ions  $2a^{+\bullet}-2f^{+\bullet}$ .

position, were protonated by electrospray ionization. The produced gas-phase ions,  $(1 + H)^+$ , were selected by mass

(m/z 530) and subjected to collision-induced dissociation (CID-MS<sup>n</sup>, Figure 1a). A sequential disassembly of the radical

Scheme 4. Proposed Dissociation Pathways of 2<sup>+•</sup>

initiator chain by CID-MS<sup>3, 29</sup> according to Scheme 1 (Figure 1b), finally produced the 5'-O-acetyl radical ion  $2^{+\bullet}$  at m/z 309 that was again selected by mass and further investigated by CID-MS<sup>4</sup> and photodissociation. CID resulted in a ribose ring cleavage that was associated with the loss of a C<sub>6</sub>H<sub>9</sub>O<sub>4</sub> radical, forming the major m/z 164 ( $C_6H_6N_5O^+$ ) fragment ion (Figure 1c). The other radical-induced dissociation was loss of C<sub>2</sub>H<sub>3</sub>O<sub>2</sub>• (m/z 250) that was accompanied by a minor loss of  $C_2H_4O_2$ (Figure 1c, inset) in a 98.6:1.4 ratio. The C<sub>2</sub>H<sub>3</sub>O<sub>2</sub>• neutral fragment was identified as an acetoxyl radical originating from the •CH2COO group. The identification was unambiguous on the basis of the CID-MS<sup>4</sup> spectrum of the  $D_5$ -ion  $2a^{+\bullet}$  that was generated from a precursor in which all exchangeable N-H and O-H protons were replaced by deuterium. The CID spectrum of  $2a^+$  (m/z 314, Figure 2a) showed a predominant loss of  $C_2H_3O_2^{\bullet}$  (m/z 255) that was accompanied by a very minor loss of  $C_2H_2DO_2^{\bullet}$  (m/z 254) in a 98.6:1.4% ratio. This excluded an alternative fragmentation by loss of a neutral radical involving the C-2' and C-3' OD groups. The loss of the acetoxyl radical necessitated a hydrogen atom migration from the ribose ring onto the CH<sub>2</sub>COO group that was further investigated by deuterium labeling. To that end, we used ions that were selectively labeled in the ribose 1', 2', 3', 4', and 5' positions,  $2b^{+\bullet}-2f^{+\bullet}$ , respectively, in addition to the H/D exchanged ion  $2a^{+\bullet}$  (Figure 2a-f). The spectra showed that neither the deuterium in positions 1', 2', and 4' nor those of the OD groups were substantially involved in the acetyl radical loss. The main channels showing deuterium transfer were from the 3' and 5' positions (Figure 2d,f, respectively). The relative intensities of the fragment ions by loss of CH<sub>3</sub>COO<sup>•</sup> and CH<sub>2</sub>DCOO<sup>•</sup> were 52:48 and 88:12 from 2d+• and 2f+•, respectively. By comparison, the deuterium transfer from C2' amounted to only 3% when based on the relative intensities for CH<sub>3</sub>COO<sup>•</sup>

and  $CH_2DCOO^{\bullet}$  loss from  $2c^{+\bullet}$ . Since no other positions were involved, the total transfer of D accounted for only 63%, indicating deuterium isotope effects. The acetoxyl radical eliminated from  $2^{+\bullet}$  may further dissociate to  $CH_3^{\bullet}$  and  $CO_2$ , as reported previously. <sup>54,55</sup>

The fragment ions produced by loss of CH3COO and CH2DCOO from 2d+ and 2f+ were further isolated and probed by CID-MS<sup>5</sup>. The spectrum of the m/z 251 ion by loss of CH<sub>3</sub>COO from 2d<sup>+</sup> showed a major fragment ion by loss of water (m/z 233, Figure S14b, Supporting Information). In contrast, the spectrum of the m/z 250 ion by loss of  $CH_2DCOO^{\bullet}$  from  $2d^{+\bullet}$  showed the formation of the m/z 164 (loss of  $C_4H_6O_2$ ) and m/z 136 ( $C_5H_6N_5^+$ ) ions (Figure S14a,b). CID-MS<sup>5</sup> of the m/z 252 (loss of CH<sub>3</sub>COO $^{\bullet}$ ) and m/z 251 (loss of CH2DCOO of from 2f of were complementary in that the former gave the m/z 164 (loss of  $C_4H_6O_2$ ) and m/z 136  $(C_5H_6N_5^+)$  ions, whereas the latter induced loss of water (Figure \$15a,b, Supporting Information). This clearly indicated that the fragment ions produced by the different mechanisms for loss of CH<sub>3</sub>COO retained distinct structures when probed by CID- $MS^5$ . The major fragment ions formed by the loss of the  $C_6H_9O_4$ radical showed a retention of three exchangeable adenine protons (m/z 167, Figure 2a) as well as 1'-D (m/z 165, Figure 2a)2b). This indicated that this major fragment ion was protonated 9-formyladenine that was produced by cleavage of the ribose C1'-C2' and C4'-O bonds. No hydrogen scrambling accompanying this dissociation was observed, as inferred from the spectra of the ions labeled in the 2' through 5' positions that showed an exclusive formation of the m/z 164 ions.

The results gained from the isotope labeling data allowed us to propose dissociation pathways for cation radical  $2^{+\bullet}$  (Scheme 4). The main pathway (3'-H) comprises a transfer of 3'-H to the acetoxyl radical, producing the 3'-radical intermediate  $3^{+\bullet}$ . The

Table 1. Relative Energies of Adenosine Cation Radicals

	U		
	relative energy <sup>a,b</sup>		
ion/reaction	M06-2X/6- 31+G(d,p)	M06-2X/aug- cc-pVTZ	CCSD(T)/6-311- +G(3df,2p)
2+•	0	0	$0 (0)^{c}$
3 <sup>+•</sup>	-11	-15	$-12(-14)^c$
6**	4	0.7	$(1)^c$
7 <sup>+•</sup>	-21	-26	$-23(-27)^c$
8+•	-14	-18	$-14(-17)^{c}$
9+•	-22	-25	$-23 (-27)^c$
10 <sup>+•</sup>	34	36	$26 (22)^c$
$TS1 \ (2^{+\bullet} \rightarrow 3^{+\bullet})$	115	117	112
$TS2 \ \big(2^{+\bullet} \to 6^{+\bullet}\big)$	147	148	139
$TS3~(2^{+\bullet} \rightarrow 8^{+\bullet})$	127	129	126
TS4 $(2^{+\bullet} \rightarrow 9^{+\bullet})$	160	157	156
$3^{+\bullet} \rightarrow TS5$	121	117	116
$3^{+\bullet} \rightarrow 11^{+\bullet}$	65	58	65
$3^{+\bullet} \rightarrow TS6$	77	76	80
$3^{+\bullet} \rightarrow 12^{+\bullet}$	-0.1	-10	-12
$2^{\bullet \bullet} \rightarrow 4^{\bullet} + C_6 H_9 O_4^{\bullet} $ $(13a^{\bullet})$	60	38	53
$3^{+\bullet} \rightarrow TS7$	105	104	105
$3^{+\bullet} \rightarrow 14^{+\bullet}$	83	83	81
$3^{+\bullet} \rightarrow TS8$	105	100	81
$3^{+\bullet} \rightarrow 15^{+\bullet}$	21	8	7
$2^{+\bullet} \rightarrow 5a^+ + $ CH <sub>3</sub> COO $^{\bullet}$	157	149	126
$2^{+\bullet} \rightarrow 5c^+ + CH_3COO^{\bullet}$	147	141	120
$6^{+\bullet} \rightarrow TS9$	73	72	
$3^{+\bullet} \to TS10$	194	193	196
$6^{^{+\bullet}} \rightarrow 16^{^{+\bullet}}$	68	67	139
$6^{ ext{+}ullet}  ightarrow 17^{ ext{+}ullet}$	42	34	
$6^{+\bullet} \rightarrow 4^{+} + C_6 H_9 O_4^{\bullet}$ $(13b^{\bullet})$	153	134	
$6^{+\bullet} \rightarrow TS11$	223	222	221
$8^{+\bullet} \rightarrow C_5 H_6 N_5^+ + C_7 H_9 O_5^{\bullet} (18^{\bullet})$	70	61	
. 1			

 $^a$ In kJ mol $^{-1}$ .  $^b$ Including B3LYP/6-31+G(d,p) zero-point vibrational energies and referring to 0 K.  $^c$ Relative Gibbs energies at 310 K.

major branch of pathway (3'-H) can proceed directly from  $3^{+\bullet}$  by consecutive cleavage of the C2'-C1' and C4'-O bonds producing the 9-formyl adenine ion  $4^+$ . Ion  $3^{+\bullet}$  can lose the acetoxyl radical via a minor pathway that involves concomitant rearrangements of the ribose ring to ions  $5a^+$  or  $5b^+$ . Upon further collisional activation, the latter isomer then can undergo a retro-Diels-Alder ring cleavage<sup>S6</sup> to form the product  $4^+$ . The alternative sequence of reactions (5'-H), indicated by the hydrogen transfer from C-5', can produce the intermediate 5'-radical  $6^{+\bullet}$  that can lose the acetoxyl radical with a concomitant rearrangement by a ribose ring oxygen migration to C-5', forming ion  $5c^+$  (Scheme 4). Ions  $5a^+$  and  $5c^+$  have C-4'-O bonds of the vinyloxide type which are not prone to dissociation, and thus, the fragmentation in the next step proceeds by loss of water.

**Ion Structures and Energies.** To substantiate the proposed dissociation pathways, we carried out extensive DFT and ab initio structure and energy calculations of isomers, transition states, intermediates, and reaction products. The calculated energies refer to the lowest-energy conformers that were obtained from BOMD trajectories and refined by DFT geometry optimizations and frequency calculations. Table 1

shows the M06-2X and CCSD(T) relative energies; the latter are discussed in text and shown in Figures and Schemes.

Isomerization of  $2^{+\bullet}$  by hydrogen migrations was found to be 12-23 kJ mol<sup>-1</sup> exothermic for the formation of the 3'-radical  $3^{+\bullet}$ , 1'-radical  $7^{+\bullet}$ , 2'-radical  $8^{+\bullet}$ , and 4'-radical  $9^{+\bullet}$  (Figure 3)

Isomerization to the 5'-radical 6<sup>+•</sup> was 3 kJ mol<sup>-1</sup> endothermic. Entropy effects slightly favored the products by 2–4 kJ mol<sup>-1</sup> (Table 1). Cation radicals 3<sup>+•</sup>, 6<sup>+•</sup>, and 7<sup>+•</sup>–9<sup>+•</sup> had the charge and radical sites in separate parts of the ion and thus satisfied the definition of distonic ions.<sup>57,58</sup> This was contrasted by the canonical 5'-O-acetyladenosine cation radical (10<sup>+•</sup>), which was less stable than the distonic isomers by up to 49 kJ mol<sup>-1</sup> when compared to the lowest-energy distonic ions 7<sup>+•</sup> and 9<sup>+•</sup>. The thermodynamic destabilization of the canonical structure can be viewed as being caused by the higher dissociation energy of the N3–H bond in 10<sup>+•</sup> relative to that of the C–H bonds in 3<sup>+•</sup>, 6<sup>+•</sup>, and 7<sup>+•</sup>–9<sup>+•</sup>. This result was consistent with a previous report of relative energies of nucleoside cation radicals favoring noncanonical distonic isomers.<sup>50,59</sup>

Transition-state structures and energies were calculated for hydrogen migrations from sterically accessible positions 3'-H (TS1), 5'-H (TS2), 2'-H (TS3), and 4'-H (TS4). TS1 (Scheme 5), which defined the hydrogen migration corresponding to the major experimentally observed channel, was a low-energy transition state at 112 kJ mol<sup>-1</sup> relative to 2<sup>+•</sup> and 124 kJ mol<sup>-1</sup> relative to 3<sup>+•</sup>. TS1 was an early transition state in which the C3'-H bond was stretched by 21% from the equilibrium position in 2<sup>+•</sup>. TS2 (Scheme 5), which corresponded to the minor channel of 5'-H migration, was at 139 and 136 kJ mol<sup>-1</sup> relative to  $2^{+\bullet}$  and  $6^{+\bullet}$ , respectively, indicating that the  $2^{+\bullet} \leftrightarrow 6^{+\bullet}$ reaction could be reversible. The other transition states, TS3 and TS4, which corresponded to the experimentally excluded migrations of 2'-H and 4'-H, respectively, (Table 1, Scheme 5), were at 126 and 156 kJ mol<sup>-1</sup> relative to  $2^{+\bullet}$ , respectively. It should be noted that alternative hydrogen atom migrations to the acetoxyl C=O were deemed to be energetically less favorable, as they would have produced high-energy enol ester isomers. For example, 3'-H atom migration to the acetoxyl C=O in 2+• was calculated to be 95 kJ mol-1 endothermic and required 178 kJ mol<sup>-1</sup> in the transition state (Scheme S2, Supporting Information). These energies indicated that ribose H atom migrations to the ester C=O were not competitive.

The further dissociation of the ribose ring was modeled by transition states for the cleavage of the C1'-C2' and C4'-O bonds. These can proceed consecutively via TS5 and TS6 (Scheme 6) or in a reverse fashion via TS7 and TS8 (Scheme 7). In the first step of the first ring-opening sequence by C1'-C2' bond dissociation, 3<sup>+•</sup> was converted to intermediate 11<sup>+•</sup> which was 65 kJ mol<sup>-1</sup> above 3<sup>+•</sup>. The TS5 energy (116 kJ mol<sup>-1</sup> above  $3^{+\bullet}$ ) indicated the possibility of reversible  $3^{+\bullet} \leftrightarrow 11^{+\bullet}$  ring opening and closure. However, the subsequent cleavage of the C4'-O bond in 11<sup>+•</sup> required a very low energy in TS6 (80 and 15 kJ mol<sup>-1</sup> relative to 3<sup>+•</sup> and 11<sup>+•</sup>, respectively) to form complex  $12^{+\bullet}$  that was at -12 kJ mol<sup>-1</sup> relative to  $3^{+\bullet}$ . When referred to  $2^{+\bullet}$ , the overall reaction sequence to  $12^{+\bullet}$  was -25 kJ mol<sup>-1</sup> exothermic. The final step, which was dissociation of complex 12<sup>+•</sup> to the formyladenine ion 4<sup>+</sup> and the dihydroxyallyl radical 13a<sup>•</sup> (Scheme 6), was overall 53 kJ mol<sup>-1</sup> endothermic relative to  $2^{+\bullet}$ .

We also investigated an alternative ring cleavage in  $3^{+\bullet}$  in which the sequence of bond-breaking reactions was reversed, such that the C4'-O bond cleavage preceded that of the C1'-

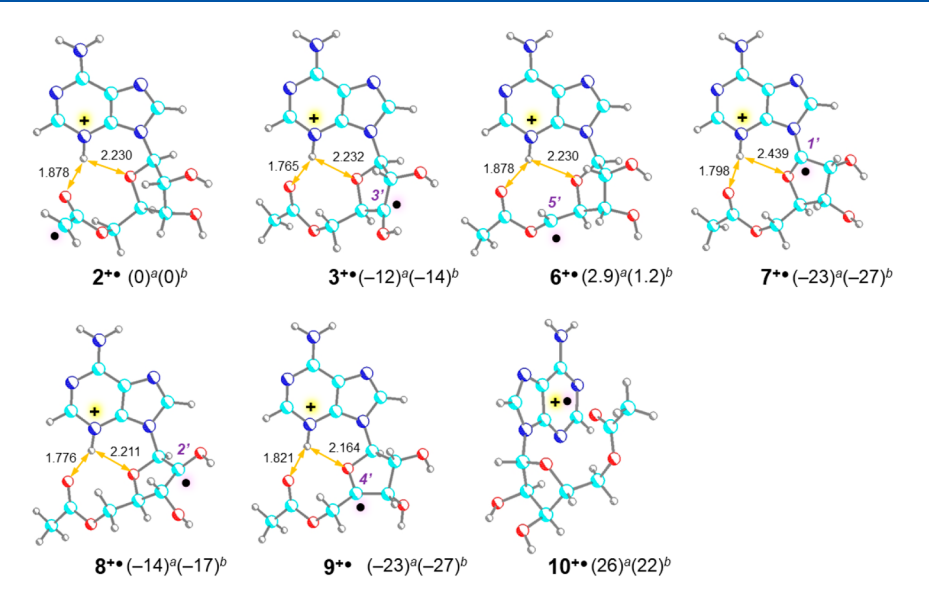
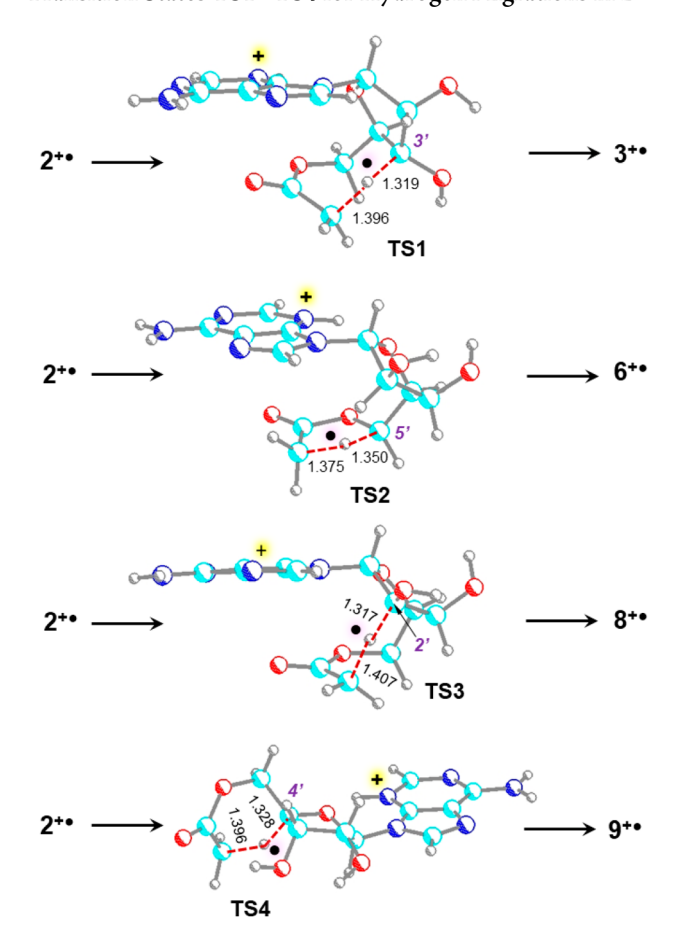


Figure 3. M06-2X/6-31+G(d,p)-optimized structures of cation radicals  $2^{+\bullet}-10^{+\bullet}$ . Atom color coding is as follows: cyan = C, gray = H, blue = N, red = O. Hydrogen bonds are shown as yellow double-headed arrows with bond lengths in Å. Relative enthalpies (<sup>a</sup>) and Gibbs energies (<sup>b</sup>) at 310 K (kJ mol<sup>-1</sup>) are from CCSD(T)/6-311++G(3df,2p) single-point calculations.

Scheme 5. M06-2X/6-31+G(d,p)-Optimized Structures of Transition States TS1-TS4 for Hydrogen Migrations in  $2^{+\bullet a}$ 



<sup>a</sup>Structure description is as in Figure 3.

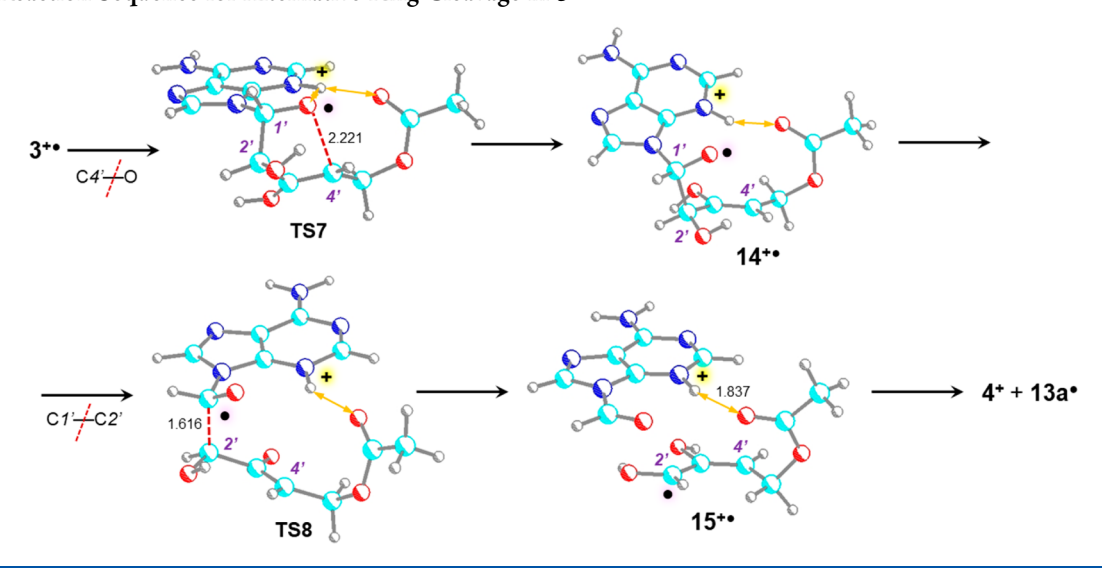
C2' bond (Scheme 7). In the first step of this reaction sequence, dissociation of the C4'-O bond proceeded via TS7 at 105 kJ mol<sup>-1</sup> above 3<sup>+•</sup>, forming intermediate 14<sup>+•</sup> at 81 kJ mol<sup>-1</sup>

(Table 1). The formed oxygen radical destabilized ion 14<sup>+•</sup>, which faced a negligible energy barrier for the consecutive dissociation of the C1′–C2′ bond through TS8 (81 kJ mol<sup>-1</sup> relative to 3<sup>+•</sup>), forming an ion–molecule complex (15<sup>+•</sup>) at 7 kJ mol<sup>-1</sup> relative to 3<sup>+•</sup>. The competition between these two ring-breaking pathways is likely to be determined by the kinetics of the first steps, which are ring openings by the C1′–C2′ and C4′–O bond dissociations proceeding via TS5 and TS7, respectively. The following ring-breaking steps had very low to negligible TS energies (TS6 and TS8) and can be expected to proceed rapidly in the respective intermediates 11<sup>+•</sup> and 14<sup>+•</sup>.

Hydrogen Migration and Dissociation Kinetics. To assess the kinetics of hydrogen migrations in 2+\*, we used the TS energies to calculate unimolecular rate constants for several channels, with the goal of evaluating the competitive dissociations observed experimentally. The experimental data were obtained for isolated ions that slowly exchanged energy with the bath helium gas, so the reaction kinetics can be considered to operate in the falloff regime. 45 We approximated the kinetics by analyzing the boundary conditions by (1) RRKM calculations for canonical rate constants applied to isolated systems and (2) transition-state theory (TST) calculations of thermal rate constants for systems undergoing fast energy exchange. We applied these methods by including primary and higher-order deuterium isotope effects and considering approximate quantum tunnel effects through parabolic barriers where the barrier width and curvature were obtained from the TS imaginary frequencies.<sup>60</sup> The RRKM rate constants for the hydrogen migration from the 2', 3', 4', and 5' positions are shown in Figure 4a. All channels for hydrogen transfer showed a substantial kinetic shift when considering the 50 ms time scale of the reactions in the ion trap. For example, hydrogen transfer from C3'  $(k_{3'-H})$ , which was the fastest reaction at internal energies up to ca. 360 kJ mol<sup>-1</sup>, required 215 kJ mol<sup>-1</sup> internal energy to proceed at 50% conversion within 50 ms, as shown by the broken line in Figure 4a. This corresponds to the kinetic shift of  $\Delta E = E_{\text{dis},50\%} - E_{\text{TS1}} = 215 - 112 = 103 \text{ kJ mol}^{-1}$ . Hydrogen transfer from C4'  $(k_{4'-H})$  was not competitive because of both its relatively high  $E_{TS4}$  (156 kJ mol<sup>-1</sup>) and a large kinetic shift,  $\Delta E =$ 

Scheme 6. Reaction Sequence for Ring Cleavage in 3+6

Scheme 7. Reaction Sequence for Alternative Ring Cleavage in 3<sup>+6</sup>



162 kJ mol<sup>-1</sup>. The rate constants for the migration from C2' and C5',  $k_{2'-H}$  and  $k_{5'-H}$ , respectively, showed a crossover at 238 kJ mol<sup>-1</sup>, which was in the kinetically relevant energy region (Figure 4a), favoring hydrogen transfer from C5' at higher internal energies. Another crossover between the competing  $k_{3'-H}$  and  $k_{5'-H}$  curves was found at 359 kJ mol<sup>-1</sup>.

The rate constants for the ring opening after the 3'-H migration ( $k_{(C4'-O)dis}$  and  $k_{(C1'-C2')dis}$ ) were substantially larger than both  $k_{3'-H}$  and the rate constant for the reverse migration ( $k_{3'-H,rev}$ ) (Figure 4b). According to the RRKM rate constants, dissociation of the C4'-O bond was the dominant reaction of  $3^{+\bullet}$  that outcompeted the alternative C1'-C2' bond cleavage across the entire kinetically relevant energy range. This also indicated that the rate-determining step for the ring cleavage and dissociation was the hydrogen migration creating the radical site at C3'.

To evaluate the competitive hydrogen migrations and compare the calculated and experimental data, we considered primary and higher-order isotope effects on the rate-determining hydrogen migration steps. The relevant rate constants and primary isotope effects  $(k_{\rm H}/k_{\rm D})$  are shown in Figures S16–S17 (Supporting Information). Secondary isotope effects were smaller. For example, the  $k_{3'\text{-H}}$  from the 5,5'-D<sub>2</sub> ion  $2f^{+\bullet}$  and 2'-D ion  $2c^{+\bullet}$  were 20–30 and 6–8% smaller, respectively, than the  $k_{3'\text{-H}}$  from  $2^{+\bullet}$ . Including the primary and higher-order isotope effects for all hydrogen and deuterium migrations allowed us to calculate the relative RRKM rate constants shown in Figure 5a–c.

The calculations showed the 3'-H migration dominating at energies up to ca.  $350 \text{ kJ mol}^{-1}$  whereby the crossover with the 5'-H curve was shifted to  $300 \text{ kJ mol}^{-1}$  for 3'-D migration due to primary isotope effects (Figure 5a). The experimental fraction of

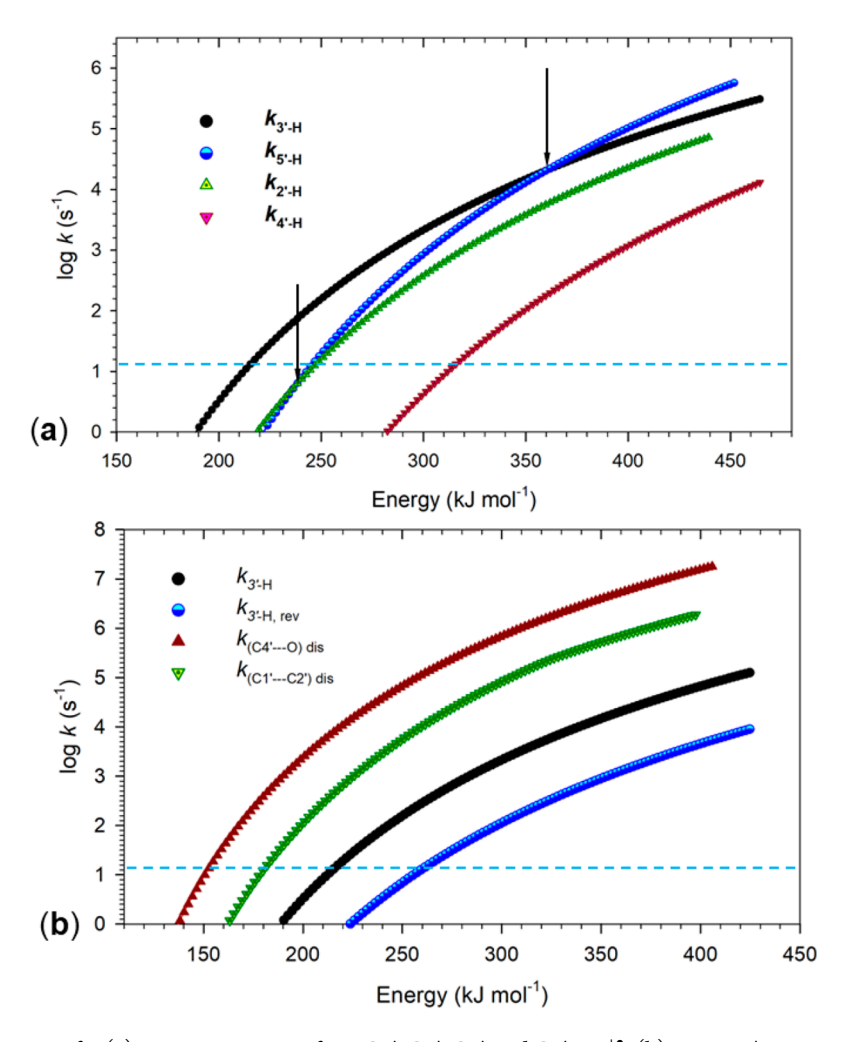
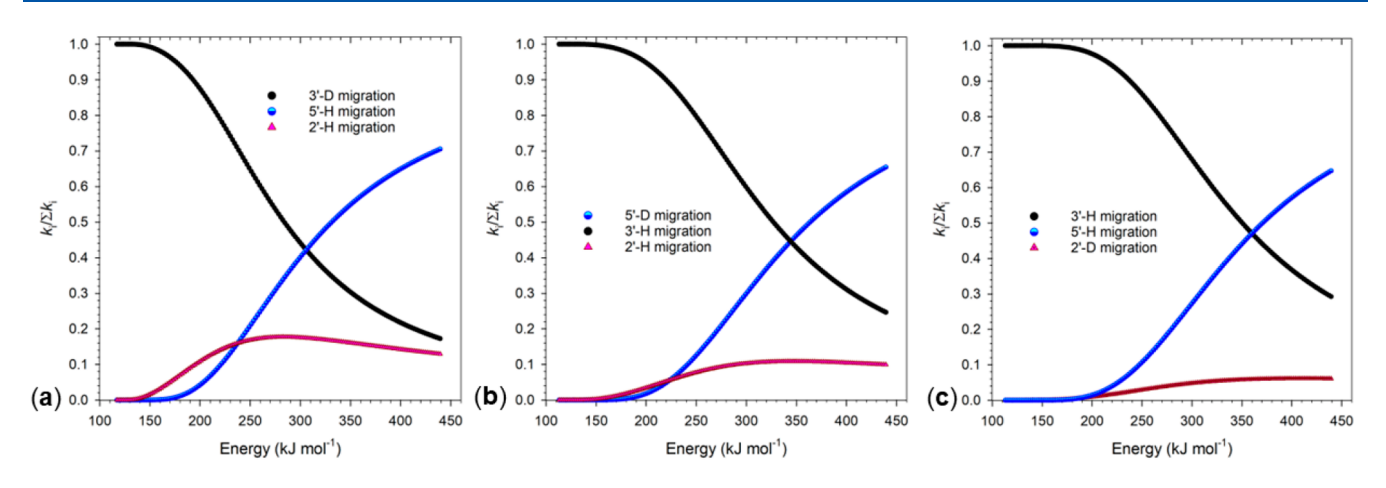


Figure 4. (a) RRKM rate constants for (a) H atom migrations from C2', C3', C4', and C5' in  $2^{+\bullet}$ ; (b) reverse 3'-H migration and ring opening in  $3^{+\bullet}$ . Calculated using CCSD(T)/6-311++G(3df,2p) + ZPVE transition-state energies. Both energy scales are relative to  $2^{+\bullet}$ . Crossovers are marked with arrows. The broken blue lines indicate rate constants allowing 50% conversion at 50 ms.



**Figure 5.** RRKM relative rate constants,  $k_i/\Sigma k_i$ , for (a) 3'-D, 2'-H, and 5'-H migrations in  $2d^{+\bullet}$ ; (b) 3'-H, 2'-H, and 5'-D migrations in  $2f^{+\bullet}$ ; (c) 3'-H, 2'-D, and 5'-H migrations in  $2c^{+\bullet}$ .

3'-D migration, 48% as inferred from the CID-MS<sup>4</sup> spectrum in Figure 2d, corresponded to the fraction of ions having ca. 270 kJ mol<sup>-1</sup> internal energy. Figure 5b showed that the migration of 5'-D was adversely affected by primary isotope effects. The experimental fraction of 5'-D migration, 12% as inferred from

Figure 2, corresponded to the fraction of ions having ca. 260 kJ  $\text{mol}^{-1}$  internal energy, which was consistent with the kinetics for the 3'-D transfer (Figure 5a). The fraction of 2'-D migration was calculated as 4–5% in the 250–270 kJ  $\text{mol}^{-1}$  energy range. This

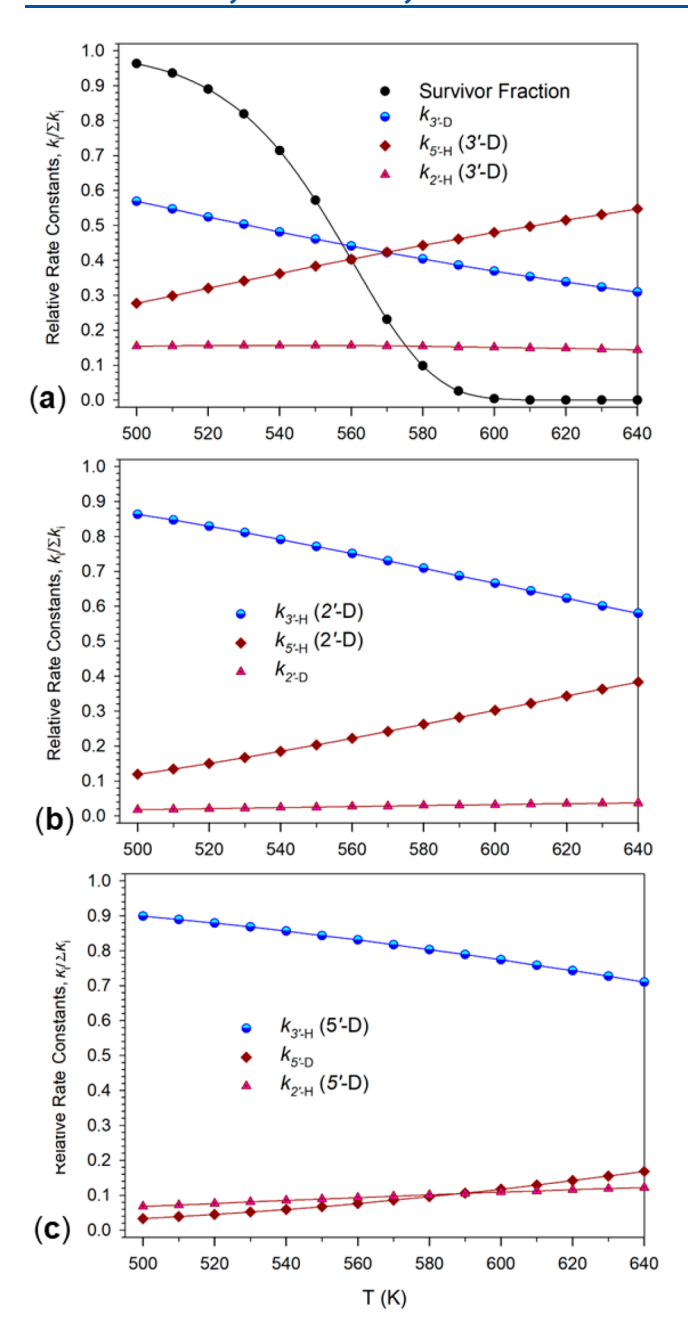


Figure 6. TST calculated relative rate constants for the migrations of (a) 3'-D, 5'-H, and 2'-H in  $2d^{+\bullet}$ , (b) 3'-H, 5'-H, and 2'-D in  $2c^{+\bullet}$ , and (c) 3'-H, 5'-D, and 2'-H in  $2f^{+\bullet}$ .

can be compared to the 3% fraction in the Figure 2c CID-MS<sup>4</sup> spectrum.

The relative rates for H transfer were also reflected by TST rate constant calculations that in addition to isotope effects also included approximate kinetic effects calculated for hydrogen and deuterium tunneling through parabolic energy barriers in TS1–TS3. The relative TST rate constants for H and D migration in  $2d^{+\bullet}$  showed 45% of 3′-D migration at the midpoint temperature of 555 K, corresponding to a 50% conversion within 50 ms (Figure 6a). This was consistent with the 48% fraction of  $CH_2DCOO^{\bullet}$  loss following 3′-D transfer. Similarly, the relative TST rate constants for  $2c^{+\bullet}$  showed 2–3% 2′-D migration (Figure 6b), which was consistent with the CID-MS<sup>4</sup> experimental data in Figure 2d. The relative TST rates for 5′-D

migration in 2f<sup>+•</sup> were 7% at 555 K and increasing at higher temperatures (Figure 6c). This was somewhat lower than the 12% estimate from the CH<sub>2</sub>DCOO loss in the Figure 2f spectrum. The rise of  $k_{5'-H}/\Sigma k_i$  and the 5'-H fraction with temperature paralleled that of the RRKM rate constants in Figure 5. This effect can be assigned to the different activation vibrational entropies in the pertinent transition states that were  $\Delta S_{TS} = -30$ , 13, and -21 J mol<sup>-1</sup> K<sup>-1</sup> for TS1, TS2, and TS3 respectively, favoring the 5'-H transfer kinetics. Tunnel effects had only a minor effect on the relative rate constants. When tunneling was ignored, the fractions for the 3'-D and 5'-D transfer increased only slightly (Figure S18, Supporting Information), indicating that these corrections were not critical for data interpretation. The calculated relative energies and rate constants showed close agreement with the experimentally observed major ring dissociation in 2+0.

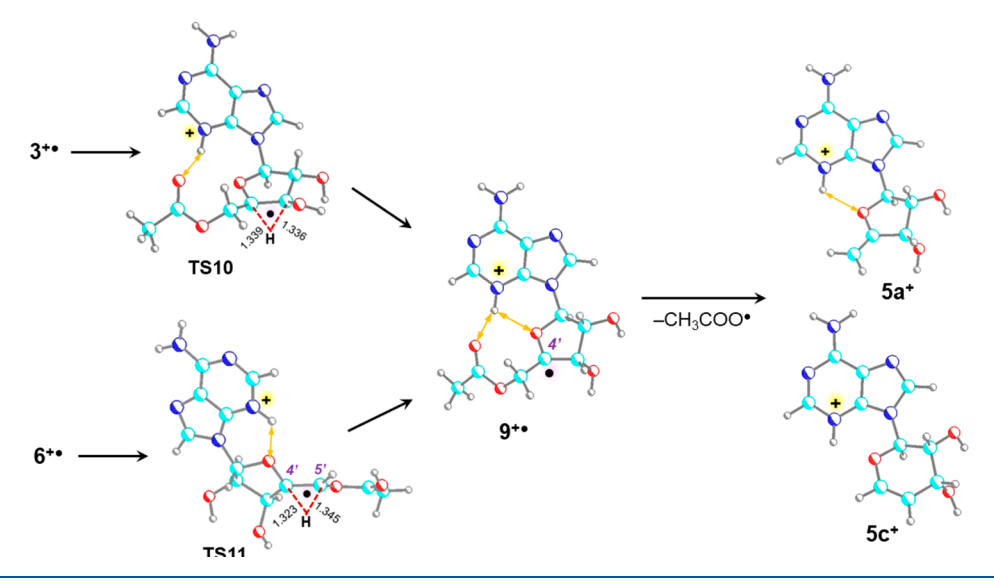
The dissociation was kinetically controlled by hydrogen atom migration from C3' that prevailed at ion energies up to ca. 360 kJ mol<sup>-1</sup>. Higher-energy ions can undergo competitive migrations from C5' and to a lesser extent from C2'. Transfer of 4'-H was kinetically uncompetitive. Following the rate-determining 3'-H transfer, the intermediate C3' radical 3<sup>+•</sup> underwent a rapid ring opening via competitive C4'-O and C1'-C2' bond dissociations. The resulting low-energy intermediates (11+ and 14+ ) exothermically dissociated to ion-molecule complexes (12+0 and 15<sup>+</sup>, respectively) before fragment separation. An alternative pathway starting from  $6^{+\bullet}$  involved ring opening by dissociation of the C4'-O bond to form intermediate 16<sup>+•</sup> via a low-energy transition state (TS9, Table 1, Scheme 8). The subsequent C1'-C2' bond dissociation in ion 16<sup>+•</sup> was 43 kJ mol<sup>-1</sup> exothermic, forming ion−molecule complex 17<sup>+•</sup>. These gas-phase reactions were driven by collisional heating of 2<sup>+•</sup> that supplied the internal energy needed for crossing the ratedetermining TS1 and TS2 (Scheme 5). However, in the condensed phase, radicals at C3' or C5' could be produced by hydrogen atom abstraction by hydroxyl radicals, which are common reactive oxygenated species (ROS) produced by water radiolysis or chemical reactions. 1,10 It is interesting to note that the predominance of 3'-H and 5'-H migration in 2+0 was consistent with the report by Khanduri et al. 11 on the formation of guanosine 3' and 5' radicals upon cation-radical photoexcitation in frozen aqueous solution.

Thus, it was of interest to investigate the dissociation kinetics of ring cleavage in  $3^{+\bullet}$  via TS7 (Scheme 7). The TST-fitted parameters for the CCSD(T)/6-311++G(3df,2p) energies were obtained as the activation energy,  $E_{\rm a}=108$  kJ mol $^{-1}$ , and frequency factor,  $\log A=13.61$ . These indicated that the ring opening in thermal  $3^{+\bullet}$  should be slow, with the rate constant of  $k=2.6\times 10^{-5}$  s $^{-1}$  at physiological 310 K. It is likely that under these conditions radical  $3^{+\bullet}$  could undergo other reactions in the condensed phase. Similar conclusions can be reached for gasphase ions stored in an ion trap, for which an average temperature of  $318\pm23$  K has been reported,  $^{61}$  again implying slow dissociation of  $3^{+\bullet}$ .

We used the loss of the acetoxyl radical in combination with specific isotope labeling as a probe of different mechanisms for H atom migration. The data showed that although hydrogen transfer is likely to trigger ring cleavage, the competing loss of the acetoxyl radical is only a minor dissociation. Another minor dissociation resulted in the formation of protonated adenine that involved four exchangeable protons, indicating proton transfer from a hydroxyl group (Figure 2a). The loss of  $CH_3COO^{\bullet}$  from  $3^{+\bullet}$  and  $6^{+\bullet}$  was expected to involve activation of the C5'-O

Scheme 8. Reaction Sequence for Ring Cleavage in 6<sup>+•</sup>

Scheme 9. Reaction Sequences for Loss of Acetoxyl Radical from 3<sup>+</sup> and 6<sup>+</sup>



bond, for example, by 1,2-hydrogen migration via TS10 and TS11, respectively, forming C4' radical  $9^{+\bullet}$  as an intermediate on the path to product ion  $5a^+$  (Scheme 9). The overall dissociation was calculated to be 126 kJ mol<sup>-1</sup> endothermic relative to 2<sup>+•</sup> (Table 1), which was consistent with this reaction competing poorly against the ring opening. In addition, the transition states for the 1,2-hydrogen migrations, TS10 and **TS11**, had high energies, 196 and 221 kJ mol<sup>-1</sup>, respectively, that should make them uncompetitive with the ring-opening reactions. We cannot exclude that the loss of CH2COO® proceeded with the involvement of other intermediates to form other products. For example, a rearrangement in  $9^{+\bullet}$  could start a pathway to the lower-energy isomer 5c<sup>+</sup>, as sketched in Scheme 2, although according to Table 1 data, the overall dissociation still had a high energy threshold of 120 kJ mol<sup>-1</sup> relative to 2<sup>+•</sup>. Because of the minor nature of this reaction, we did not pursue it further.

The formation of the protonated adenine ion can be visualized by the reaction sequence shown in Scheme 8. Starting from 2'-

radical  $8^{+\bullet}$ , cleavage of the C1′–N9 bond is followed by a hydrogen transfer from a hydroxyl group onto the adenine cation radical, forming N3-protonated adenine and radical  $18^{\bullet}$ . Although we did not investigate the mechanistic details of this dissociation, its low thermochemical threshold (61 kJ mol<sup>-1</sup> relative to  $8^{+\bullet}$ ) may favor it.

**UV–Vis Action Spectroscopy.** With regard to the reaction kinetics for the hydrogen migrations in  $2^{+\bullet}$ , it was of interest to probe the structure of the ions generated in the ion trap. According to Scheme 1, the acetoxyl radical  $2^{+\bullet}$  was produced by CID-MS<sup>n</sup> of its precursor ion  $(1 + H)^+$  that could lead to vibrational excitation, possibly driving exothermic hydrogen atom migrations. In contrast, for  $2^{+\bullet}$  thermalized to the presumed range of ion trap storage temperatures (318-355 K), the rate constants for the 3'-H migration  $(k_{3'-H} = 1.5 \times 10^{-7}-1.3\times 10^{-5} \, \text{s}^{-1})$  would prevent isomerization during the 50 ms residence time. To further address this issue experimentally, we used photodissociation action spectroscopy to probe the ion absorption in the  $210-700 \, \text{nm}$  region. The action spectrum was

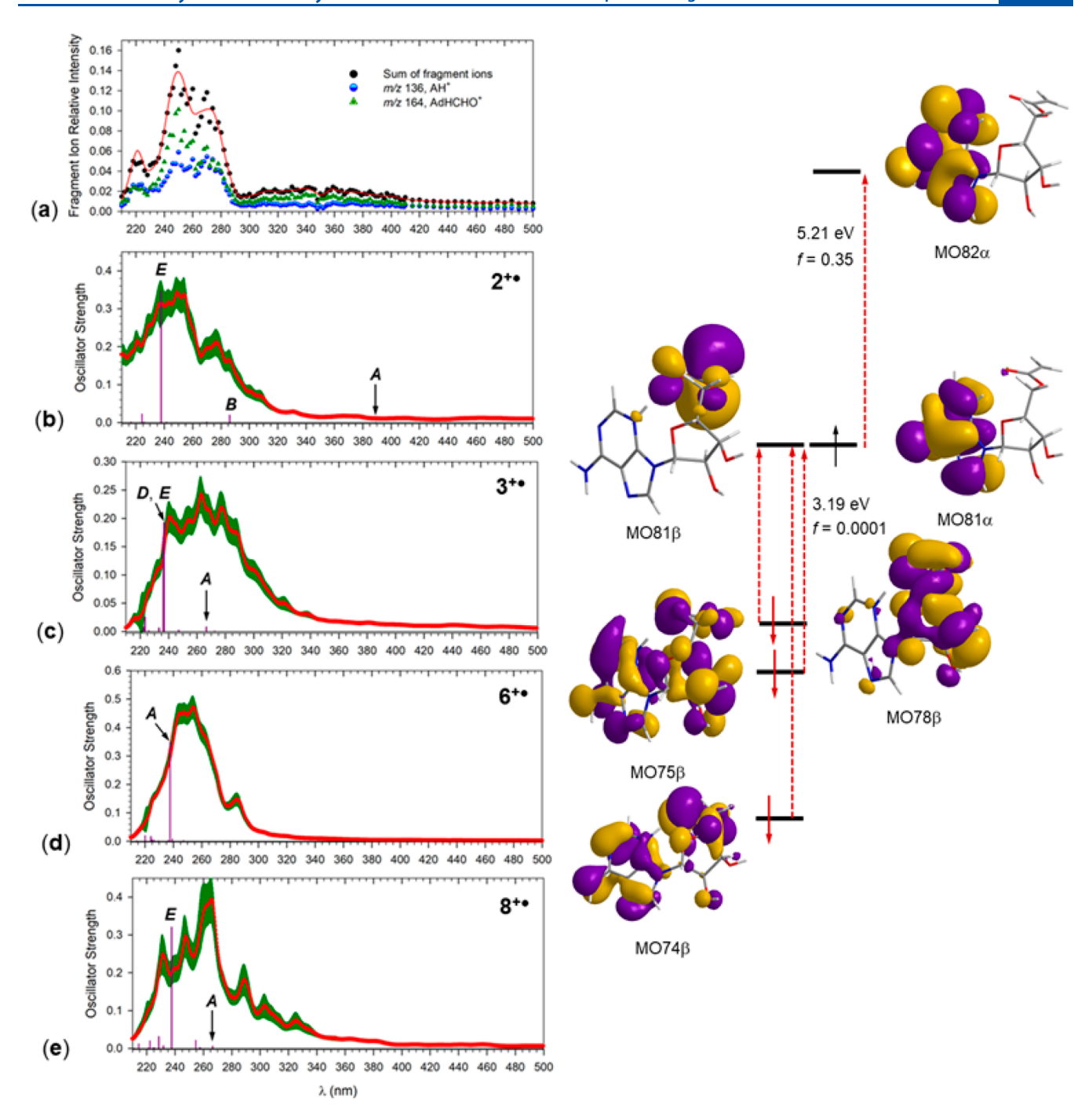


Figure 7. Left panel: (a) UV—vis action spectrum of  $2^{+\bullet}$ . (b—e) M06-2X/6-31+G(d,p) calculated vibronic absorption spectra of  $2^{+\bullet}$ ,  $3^{+\bullet}$ ,  $6^{+\bullet}$ , and  $8^{+\bullet}$ . Right panel: Molecular orbital representation of electron excitations in  $2^{+\bullet}$  leading to the A and E states.

monitored at the m/z 164 and 136 fragment ion channels (Figure 7a, left panel). The spectrum showed a weak broad band centered at 360 nm and three bands with maxima at 270, 250, and 220 nm. There was no absorption above 500 nm that would result in photodissociation. The action spectrum was compared to the calculated vibronic spectra of ions  $2^{+\bullet}$ ,  $3^{+\bullet}$ ,  $6^{+\bullet}$ , and  $8^{+\bullet}$  (Figure 7b-e) as well as those of the less likely isomers  $7^{+\bullet}$ ,  $9^{+\bullet}$ , and  $10^{+\bullet}$  (Figure S19, Supporting Information). The calculated spectra showed common  $\pi_z \to \pi_z^*$  transitions at 230–240 nm that appeared as vibronic bands at 240–260 nm, matching the major 250 nm band in the action spectrum. The main difference between the vibronic spectra of  $2^{+\bullet}$ ,  $3^{+\bullet}$ ,  $6^{+\bullet}$ , and  $8^{+\bullet}$  was the

weak band at 370 nm that was present only for  $2^{+\bullet}$ . This band arose by electron transition to the first excited state (A) that had a low oscillator strength, f = 0.0001, in the ground vibrational state of  $2^{+\bullet}$  but was enhanced in configurations produced by vibrational excitation at 310–350 K. The electron transitions to the A state were found to involve internal excitations to the singly occupied molecular orbital (MO81) from the underlying MO74, MO75, and MO78 within the  $\beta$ -electron manifold (Figure 7, right panel). These orbitals were delocalized over the acetyloxy group, ribose oxygens, and adenine and can be considered to be sensitive to conformational changes due to vibrational excitation. Overall, the vibronic spectrum of  $2^{+\bullet}$ 

Table 2. Relative Energies of  $\mathbf{2}'$ -Deoxyadenosine Cation Radicals

	relative energy <sup>a,b</sup>		
ion/reaction	M06-2X/6- 31+G(d,p)	M06-2X/aug-cc- pVTZ	$\Delta E^c$
d2 <sup>+</sup> •	0	$0 (0)^d$	0
d3 <sup>+•</sup>	-17	$-18(-22)^{d}$	-3
d6 <sup>+•</sup>	2.7	$-0.3 (-3.1)^d$	-1
d7 <sup>+•</sup>	-22	$-26 (-30)^d$	-0.7
d8 <sup>+</sup> •	10	$7.7 (4.0)^d$	26
d9 <sup>+•</sup>	-21	$-25 (-30)^d$	0.5
d10 <sup>+•</sup>	43	$44 (22)^d$	7.9
$TSd1\ (d2^{+\bullet} \to d3^{+\bullet})$	106	109	-8
$TSd2\ (d2^{+\bullet} \to d6^{+\bullet})$	141	144	-4
$TSd3 \ (d2^{+\bullet} \rightarrow d8^{+\bullet})$	139	142	13
$TSd4 \left( d2^{+\bullet} \rightarrow d9^{+\bullet} \right)$	165	162	5
$d3^{+\bullet} \rightarrow 4^+ + C_6 H_9 O_4^{\bullet}$ $(d13a^{\bullet})$	103	86	48
$d3^{+\bullet} \rightarrow TSd5$	137	130	13
$d3^{+\bullet} \to d11^{+\bullet}$	75	66	8
$d3^{+\bullet} \to d12^{+\bullet}$	25	13	24
$d3^{+\bullet} \rightarrow TSd7$	89	89	-16
$d3^{+\bullet} \rightarrow d14^{+\bullet}$	71	69	-14
$d3^{+\bullet} \rightarrow TSd8$	87	84	-16
$d6^{+\bullet} \rightarrow TSd9$	83	83	10
$d6^{+\bullet} \rightarrow d16^{+\bullet}$	79	78	11
$d6^{+\bullet} \rightarrow 4^{+} + C_6 H_9 O_4^{\bullet}$ $(d13b^{\bullet})$	176	160	26

"In kJ  $\mathrm{mol}^{-1}$ . "Including B3LYP/6-31+G(d,p) zero-point vibrational energies and referring to 0 K. "Relative to the analogous M06-2X/aug-cc-pVTZ entry for adenosine cation radicals in Table 1. "Relative Gibbs energies at 310 K.

showed the best match with the action spectrum, considering the bands at 280 and 220–225 nm in addition to the 250 and 360 nm bands. This allowed us to conclude that the probed hydrogen migrations were not proceeding spontaneously in  $2^{+\bullet}$  upon its formation but were driven by collisional activation in the next CID-MS<sup>n</sup> step.

Relative Energies of 5-Acetyl-2'-deoxyadenosine **Cation Radicals.** The results of the energy and kinetic analysis of adenosine cation radicals raised the question of analogous reactions in 2'-deoxyadenosine ions when triggered by the 5'acetoxyl radical handle. The energetics of 2'-deoxyadenosine cation-radical reactions were evaluated from M06-2X/aug-ccpVTZ single-point energies, for the data for the adenosine system indicated that the M06-2X and CCSD(T) energies followed the same trends (Table 1). The deoxyadenosine ions corresponding to their adenosine analogues are denoted as d2<sup>+</sup>, d3<sup>+•</sup>, etc.; the transition states are labeled accordingly as TSd1, TSd2, etc. The deoxyadenosine ion structures and relative energies are shown in Schemes S3-S5 (Supporting Information) and compiled in Table 2. The relative energies of the acetoxyl  $(d2^{+\bullet})$ , 1'  $(d7^{+\bullet})$ , 4'  $(d9^{+\bullet})$ , and 5'  $(d6^{+\bullet})$  radicals closely followed the same series of adenosine radicals, with differences in relative energies between the two series being within 1 kJ mol<sup>-1</sup>. The 3'-radical (d3<sup>+•</sup>) was slightly stabilized compared to  $3^{+•}$  ( $\Delta E = -3$  kJ mol<sup>-1</sup>), whereas the canonical cation radical (d10<sup>+•</sup>) was destabilized compared to 10<sup>+•</sup> (Table 2). The largest effect was the 26 kJ mol<sup>-1</sup> destabilization of the 2'-radical d8<sup>+•</sup> compared to 8<sup>+•</sup>, indicating that the 2-hydroxyl group had an energy-lowering effect on the  $\alpha$ -radical at C2'. It is noteworthy that in contrast to 2'-deoxyadenosine cation

radicals, the relative energies in 2'-deoxyribose radicals have been reported to follow the series of  $\Delta H_{0,g}$  C5' < C4'  $\approx$  C3' < C1' < C2', favoring the radical at C5'. The transition states for the hydrogen transfer showed minor energy-lowering effects on the transfer of 3'-H (TSd1,  $\Delta E = -8 \text{ kJ mol}^{-1}$ ) and 5'-H (TSd2,  $\Delta E = -4 \text{ kJ mol}^{-1}$  Scheme S3, Table 2), contrasting a 13 kJ mol<sup>-1</sup> energy increase in TSd3 for the 2'-H transfer (Scheme S4). The pertinent transition states showed minor differences in geometry and spin densities. TS3 was an early transition state in which the C2'-H bond was extended to 1.317 Å, and C2' carried 37% of spin density with additional 6% allocated to the 2'-oxygen. In contrast, TSd3 was a late transition state in which the C2'-H bond was extended to 1.371 Å, and C2' carried 49% of spin density. This correlated with the reaction thermochemistry where the formation of 8<sup>+•</sup> and d8<sup>+•</sup> was exo- and endothermic, respectively.

Differences were also found in the thermodynamics and TS energies of the ring cleaving reactions (Scheme S5, Table 2). The ring-opening reaction breaking the C4′-O bond in the 3′radical  $(d3^{+\bullet})$  had a lower energy  $(TSd7, 89 \text{ kJ mol}^{-1})$  than the analogous reaction in 3<sup>+•</sup> (TS7, 104 kJ mol<sup>-1</sup>). In contrast, breaking the C1'-C2' bond in  $d3^{+\bullet}$  (TSd5, 130 kJ mol<sup>-1</sup>) was less favorable than the analogous reaction in 3<sup>+•</sup> with TS5 at 117 kJ mol-1 at the same level of theory. These differences can further favor the C4'-O bond dissociation route in d3<sup>+•</sup>. A similar lowering of TS energy was found for TSd7 versus TS7  $(\Delta E = -16 \text{ kJ mol}^{-1})$  that overall indicated a higher propensity of the 2'-deoxyribose ring to radical-initiated cleavage. This effect can be mitigated by the energy for the overall dissociation, which was higher for d3<sup>+•</sup> than for 3<sup>+•</sup>, 86 and 38 kJ mol<sup>-1</sup>, respectively. This difference can be ascribed to the greater stabilization by  $\pi$ -electron conjugation in radical 13a $^{\bullet}$  (Scheme 6) when compared with d13a<sup>•</sup> (Scheme S5).

## CONCLUSIONS

The experimental data and calculations reported here pointed to the formation of adenine-protonated 5'-O-acetoxyladenosine radicals upon collision-induced dissociation, as corroborated by UV-vis action spectroscopy. Further collisional activation of the cation radical drove intramolecular hydrogen atom migrations that chiefly involved the sterically accessible 3'-H with minor contributions from 5'-H and 2'-H. The migrations were controlled kinetically, not by the reaction thermochemistry, and triggered further ribose cross-ring cleavage. Calculations of the 5'-O-acetoxyl-2'-deoxyadenosine cation radicals showed that the C2' radical was thermochemically and kinetically destabilized relative to the same position in riboadenosine, pointing to a lower reactivity toward radical attack at C2' in 2'deoxyadenosine. When sugar radicals were produced at C3' by hydrogen atom abstraction, both the ribose and 2'-deoxyribose rings can undergo facile cleavage by C4'-O and C1'-C2' bond dissociations. The calculated transition-state energies indicated that the ring cleavage was more facile in 2'-deoxyribose radicals.

# ASSOCIATED CONTENT

#### Supporting Information

The Supporting Information is available free of charge at https://pubs.acs.org/doi/10.1021/acs.jpca.3c07906.

Description of synthetic procedures with compound spectroscopic characterization, additional figures including NMR and mass spectra, reaction schemes and energies from DFT calculations (PDF)

### AUTHOR INFORMATION

## **Corresponding Author**

František Tureček — Department of Chemistry, University of Washington, Seattle, Washington 98195-1700, United States; Phone: +1-206-685-2041; Email: turecek@uw.edu

#### **Authors**

Václav Zima — Department of Chemistry, University of Washington, Seattle, Washington 98195-1700, United States; Institute of Organic Chemistry and Biochemistry, Czech Academy of Sciences, 166 10 Prague 6, Czech Republic

Aleš Marek — Institute of Organic Chemistry and Biochemistry, Czech Academy of Sciences, 166 10 Prague 6, Czech Republic;

orcid.org/0000-0001-9031-8263

Complete contact information is available at: https://pubs.acs.org/10.1021/acs.jpca.3c07906

#### Notes

The authors declare no competing financial interest.

## ACKNOWLEDGMENTS

Support by the Chemistry Division of the U.S. National Science Foundation (Grant CHE-1951518) and the Klaus and Mary Ann Saegebarth Endowment is gratefully acknowledged. Research at the IOCB was supported by the Ministry of Education, Youth and Sport (MSMT INTER-EXCELLENCE LTAUSA19094).

## REFERENCES

- (1) von Sonntag, C. Free-Radical-Induced DNA Damage and Its Repair; Springer, 2006.
- (2) Äyene, I. S.; Koch, C. J.; Krisch, R. E. Role of Scavenger-Derived Radicals in the Induction of Double-Strand and Single-Strand Breaks in Irradiated DNA. *Radiat. Res.* **1995**, *142*, 133–143.
- (3) Nayek, U.; Unnikrishnan, V. K.; Abdul Salam, A. A.; Chidangil, S.; Mathur, D. Thermal Energy Electrons and OH-Radicals Induce Strand Breaks in DNA in an Aqueous Environment: Some Salts Offer Protection Against Strand Breaks. *J. Phys. Chem. A* **2020**, *124*, 1508–1514.
- (4) Sanche, L. Low Energy Electron-Driven Damage in Biomolecules. *Eur. Phys. J. D Atomic, Molecular, Optical and Plasma Physics* **2005**, 35, 367–390.
- (5) Alizadeh, E.; Orlando, T. M.; Sanche, L. Biomolecular Damage Induced by Ionizing Radiation: the Direct and Indirect Effects of Low-Energy Electrons on DNA. *Annu. Rev. Phys. Chem.* **2015**, *66*, 379–398.
- (6) Peoples, A. R.; Mercer, K. R.; Bernhard, W. A. What Fraction of DNA Double-Strand Breaks Produced by the Direct Effect is Accounted for by Radical Pairs? *J. Phys. Chem. B* **2010**, *114*, 9283–9288.
- (7) Gu, J.; Wang, J.; Leszczynski, J. Electron Attachment-Induced DNA Single Strand Breaks: C3'-O3' σ-Bond Breaking of Pyrimidine Nucleotides Predominates. *J. Am. Chem. Soc.* **2006**, *128*, 9322–9323.
- (8) Gu, J.; Wang, J.; Leszczynski, J. Electron Attachment-Induced DNA Single-Strand Breaks at the Pyrimidine Sites. *Nucleic Acids Res.* **2010**, 38, 5280–5290.
- (9) Burrows, C. J.; Muller, J. G. Oxidative Nucleobase Modifications Leading to Strand Scission. *Chem. Rev.* **1998**, 98, 1109–1151.
- (10) Knapp Pogozelski, W.; Tullius, T. D. Oxidative Strand Scission of Nucleic Acids: Routes Initiated by Hydrogen Abstraction from the Sugar Moiety. *Chem. Rev.* **1998**, *98*, 1089–1108.
- (11) Khanduri, D.; Collins, S.; Kumar, A.; Adhikary, A.; Sevilla, M. D. Formation of Sugar Radicals in RNA Model Systems and Oligomers via Excitation of Guanine Cation Radical. *J. Phys. Chem. B* **2008**, *112*, 2168–2178.

- (12) Miaskiewicz, K.; Osman, R. Theoretical Study on the Deoxyribose Radicals Formed by Hydrogen Abstraction. *J. Am. Chem. Soc.* **1994**, *116*, 232–238.
- (13) Colson, A.-O.; Sevilla, M. D. Structure and Relative Stability of Deoxyribose Radicals in a Model DNA Backbone: Ab Initio Molecular Orbital Calculations. *J. Phys. Chem.* **1995**, *99*, 3867–3874.
- (14) Wetmore, S. D.; Boyd, R. J.; Eriksson, L. A. A Comprehensive Study of Sugar Radicals in Irradiated DNA. *J. Phys. Chem. B* **1998**, *102*, 7674–7686.
- (15) Taverna Porro, M. L.; Greenberg, M. M. DNA double strand cleavage via interstrand hydrogen atom abstraction. *J. Am. Chem. Soc.* **2013**, *135*, 16368–16371.
- (16) Ramirez-Arizmendi, L. E.; Heidbrink, J. L.; Guler, L. P.; Kenttamaa, H. I. Reactivity of Substituted Charged Phenyl Radicals Toward Components of Nucleic Acids. *J. Am. Chem. Soc.* **2003**, 125, 2272–2281.
- (17) Turecek, F. Flying DNA Cation Radicals in the Gas Phase: Generation and Action Spectroscopy of Canonical and Noncanonical Nucleobase Forms. *J. Phys. Chem. B* **2021**, *125*, 7090–7100.
- (18) Korn, J. A.; Urban, J.; Dang, A.; Nguyen, H. T. H.; Turecek, F. UV-Vis Action Spectroscopy Reveals a Conformational Collapse in Hydrogen-Rich Dinucleotide Cation Radicals. *J. Phys. Chem. Lett.* **2017**, *8*, 4100–4107.
- (19) Liu, Y.; Korn, J. A.; Dang, A.; Turecek, F. Hydrogen-Rich Cation Radicals of DNA Dinucleotides. Generation and Structure Elucidation by UV-Vis Action Spectroscopy. *J. Phys. Chem. B* **2018**, *122*, 9665–9680.
- (20) Liu, Y.; Korn, J. A.; Turecek, F. UV-Vis Action Spectroscopy and Structures of Hydrogen-Rich 2'-Deoxycytidine Dinucleotide Cation Radicals. A Difficult Case. *Int. J. Mass Spectrom.* **2019**, 443, 22–31.
- (21) Huang, S. R.; Liu, Y.; Tureček, F. UV-Vis Photodissociation Action Spectroscopy Reveals Cytosine-Guanine Hydrogen Transfer in DNA Tetranucleotide Cation Radicals upon One-Electron Reduction. *J. Phys. Chem. B* **2020**, *124*, 3505–3517.
- (22) Liu, Y.; Huang, S. R.; Tureček, F. Guanine-Adenine Interactions in DNA Tetranucleotide Cation Radicals Revealed by UV/Vis Photodissociation Action Spectroscopy and Theory. *Phys. Chem. Chem. Phys.* **2020**, *22*, 16831–16842.
- (23) Wan, J.; Brož, B.; Liu, Y.; Huang, S. R.; Marek, A.; Tureček, F. The DNA Radical Code. Resolution of Identity in Dissociations of Trinucleotide Cation Radicals in the Gas Phase. *J. Am. Soc. Mass Spectrom.* **2023**, *34*, 304–319.
- (24) Tureček, F. UV-Vis Spectroscopy of Gas-Phase Ions. *Mass Spectrom. Rev.* **2023**, 42, 206–226.
- (25) Feketeova, L.; Chan, B.; Khairallah, G. N.; Steinmetz, V.; Maitre, P.; Radom, L.; O'Hair, R. A. J. Watson-Crick Base Pair Radical Cation as a Model for Oxidative Damage in DNA. *J. Phys. Chem. Lett.* **2017**, *8*, 3159–3165.
- (26) Hodyss, R.; Cox, H. A.; Beauchamp, J. L. Bioconjugates for Tunable Peptide Fragmentation: Free Radical Initiated Peptide Sequencing (FRIPS). J. Am. Chem. Soc. 2005, 127, 12436–12437.
- (27) Desai, N.; Thomas, D. A.; Lee, J.; Gao, J.; Beauchamp, J. L. Eradicating Mass Spectrometric Glycan Rearrangement by Utilizing Free Radicals. *Chem. Sci.* **2016**, *7*, 5390–5397.
- (28) Zimnicka, M.; Moss, C. L.; Chung, T. W.; Hui, R.; Tureček, F. Tunable Charge Tags for Electron-Based Methods of Peptide Sequencing. Design and Applications. *J. Am. Soc. Mass Spectrom.* **2012**, 23, 608–620.
- (29) Zima, V.; Liu, Y.; Tureček, F. Radical Cascade Dissociation Pathways to Unusual Nucleobase Cation Radicals. *J. Am. Soc. Mass Spectrom.* **2022**, 33, 1038–1047.
- (30) Dang, A.; Korn, J. A.; Gladden, J.; Mozzone, B.; Tureček, F. UV-Vis Photodissociation Action Spectroscopy on Thermo LTQ-XL ETD and Bruker amaZon Ion Trap Mass Spectrometers: A Practical Guide. *J. Am. Soc. Mass Spectrom.* **2019**, *30*, 1558–1564.
- (31) Řezáč, J. Cuby: An Integrative Framework for Computational Chemistry. J. Comput. Chem. 2016, 37, 1230–1237.

- (32) Stewart, J. J. P. Optimization of Parameters for Semi-Empirical Methods. V. Modification of NDDO Approximations and Application to 70 Elements. *J. Mol. Model.* **2007**, *13*, 1173–1213.
- (33) Řezáč, J.; Fanfrlík, J.; Salahub, D.; Hobza, P. Semi-Empirical Quantum Chemical PM6Method Augmented by Dispersion and H Bonding Correction Terms Reliably Describes Various Types of Noncovalent Complexes. J. Chem. Theory Comput. 2009, 5, 1749–1760.
- (34) Stewart, J. J. P. MOPAC 16; Stewart Computational Chemistry: Colorado Springs, CO, 2016.
- (35) Berendsen, H. J.; Postma, J. V.; van Gunsteren, W. F.; DiNola, A. R. H. J.; Haak, J. R. Molecular Dynamics with Coupling to an External Bath. *J. Chem. Phys.* **1984**, *81*, 3684–3690.
- (36) Becke, A. D. Density-Functional Exchange-Energy Approximation with Correct Asymptotic Behavior. *Phys. Rev. A* **1988**, *38*, 3098–3100.
- (37) Zhao, Y.; Truhlar, D. G. The M06 Suite of Density Functionals for Main Group Thermochemistry, Thermochemical Kinetics, Noncovalent Interactions, Excited States, and Transition Elements: Two New Functionals and Systematic Testing of Four M06-Class Functionals and 12 Other Functionals. *Theor. Chem. Acc.* 2008, 120, 215–241.
- (38) Dunning, T. H., Jr Gaussian Basis Sets for Use in Correlated Molecular Calculations. I. The Atoms Boron Through Neon and Hydrogen. J. Chem. Phys. 1989, 90, 1007–1023.
- (39) Weigend, F.; Ahlrichs, R. Balanced Basis Sets of Split Valence, Triple Zeta Valence and Quadruple Zeta Valence Quality for H to Rn. Design and Assessment of Accuracy. *Phys. Chem. Chem. Phys.* **2005**, *7*, 3297–3305.
- (40) Weigend, F. Accurate Coulomb-Fitting Basis Sets for H to Rn. *Phys. Chem. Chem. Phys.* **2006**, *8*, 1057–1065.
- (41) Møller, C.; Plesset, M. S. A Note on an Approximation Treatment for Many-Electron Systems. *Phys. Rev.* **1934**, *46*, 618–622.
- (42) Čížek, J. On the Use of the Cluster Expansion and the Technique of Diagrams in Calculations of Correlation Effects in Atoms and Molecules. *Adv. Chem. Phys.* **1969**, *14*, 35–89.
- (43) Purvis, G. D., III; Bartlett, R. J. A. Full Coupled-Cluster Singles and Doubles Model the Inclusion of Disconnected Triples. *J. Chem. Phys.* **1982**, *76*, 1910–1918.
- (44) Curtiss, L. A.; Raghavachari, K.; Pople, J. A. Gaussian-2 Theory Using Reduced Moller-Plesset Orders. *J. Chem. Phys.* **1993**, *98*, 1293–1298.
- (45) Gilbert, R. G.; Smith, S. C. Theory of Unimolecular and Recombination Reactions; Blackwell Scientific Publications: Oxford, 1990; pp 52–132.
- (46) Zhu, L.; Hase, W. L. Quantum Chemistry Program Exchange, Program No. QCPE 644; Indiana University: Bloomington, IN, 1994.
- (47) Frank, A. J.; Sadílek, M.; Ferrier, J. G.; Turecek, F. Sulfur Oxoacids and Radicals in the Gas Phase. A Variable-Time Neutralization-Photoexcitation-Reionization Mass Spectrometric and Ab initio/RRKM Study. J. Am. Chem. Soc. 1997, 119, 12343–12353.
- (48) Furche, F.; Ahlrichs, A. Adiabatic Time-Dependent Density Functional Methods for Excited State Properties. *J. Chem. Phys.* **2002**, 117, 7433–7447.
- (49) Turecek, F. Benchmarking Electronic Excitation Energies and Transitions in Peptide Radicals. *J. Phys. Chem. A* **2015**, *119*, 10101–10111.
- (50) Huang, S. R.; Dang, A.; Tureček, F. Ground and Excited States of Gas-Phase DNA Nucleobase Cation-Radicals. A UV-Vis Photodissociation Action Spectroscopy and Computational Study of Adenine and 9-Methyladenine. J. Am. Soc. Mass Spectrom. 2020, 31, 1271–1281.
- (51) Wigner, E. On The Quantum Correction for Thermodynamic Equilibrium. *Phys. Rev.* **1932**, *40*, 749–759.
- (52) Bonacić-Koutecký, V.; Mitrić, R. Theoretical Exploration of Ultrafast Dynamics in Atomic Clusters: Analysis and Control. *Chem. Rev.* 2005, 105, 11–66.
- (53) Barbatti, M.; Ruckenbauer, M.; Plasser, F.; Pittner, J.; Granucci, G.; Persico, M.; Lischka, H. Newton-X: A Surface-Hopping Program

- for Nonadiabatic Molecular Dynamics. Wiley Interdisciplinary Reviews: Comput. Mol. Sci. 2014, 4, 26–33.
- (54) Schröder, D.; Soldi-Lose, H.; Schwarz, H. Unimolecular Rearrangements of Transient Carboxy Radicals and Cations. *Aust. J. Chem.* **2003**, *56*, 443–451.
- (55) Lu, Z.; Continetti, R. E. Dynamics of the Acetoxyl Radical Studied by Dissociative Photodetachment of the Acetate Anion. *J. Phys. Chem. A* **2004**, *108*, 9962–9969.
- (56) Tureček, F.; Hanuš, V. The Retro-Diels-Alder Reaction in Mass Spectrometry. *Mass Spectrom. Rev.* **1984**, *3*, 85–152.
- (57) Yates, B. F.; Bouma, W. J.; Radom, L. Distonic Radical Cations Guidelines for the Assessment of Their Stability. *Tetrahedron* **1986**, *42*, 6225–6234.
- (58) Hammerum, S. Distonic Radical Cations in Gaseous and Condensed Phase. *Mass Spectrom. Rev.* **1988**, *7*, 123–202.
- (59) Huang, S. R.; Tureček, F. Non-Canonical DNA Nucleoside Cation Radicals. A Computational Study of the Dark Matter of DNA Ionization. *J. Phys. Chem. B* **2022**, *126*, 2480–2497.
- (60) Bell, R. P. The Tunnel Effect in Chemistry; Chapman and Hill: London, 1980; pp 21–26, 60–62.
- (61) Donald, W. A.; Khairallah, G. N.; O'Hair, R. A. J. The Effective Temperature of Ions Stored in a Linear Quadrupole Ion Trap Mass Spectrometer. *J. Am. Soc. Mass Spectrom.* **2013**, *24*, 811–815.
- (62) Vannier, L. A.; Yao, C.; Tureček, F. 2-Deoxyribose Radicals in the Gas Phase and Aqueous Solution. Transient Intermediates of Hydrogen Atom Abstraction from 2-Deoxyribofuranose. *Collect. Czech. Chem. Commun.* **2005**, *70*, 1769–1786.